

Multiscale simulation of surface roughening of a deep drawing steel due to subsurface plastic deformation

Aiden Carley-Clopton^{1*}, Grethe Winther¹, Oleg V. Mishin¹, and Chris Valentin Nielsen¹

¹ Department of Civil and Mechanical Engineering, Technical University of Denmark, Kongens Lyngby, Denmark

Abstract. Surface roughness due to plastic deformation is important as it impacts both the surface properties of finished parts and tribological conditions during metal forming. In the present study, an approach for modeling free surface roughening due to the heterogeneous microstructure of polycrystals, where grains deform differently, is presented and validated experimentally for uniaxial tension. Roughening is modelled by finite element crystal plasticity simulations. Two methods of applying boundary conditions to the polycrystal are used. One method involves multi-scale modeling, where the continuum-scale simulation provides the submodel boundary conditions. In the second method, the elongation is applied directly by a moving periodic boundary. Material properties of DC04 steel sheet are measured by uniaxial tensile testing. Microstructure is characterized by optical microscopy and electron backscatter diffraction is used as input to generate representative simulation models. Material parameters for crystal plasticity are determined by matching simulation results to experimental stress-strain behavior. Experimental surface topography measurements by confocal microscopy after deformation are presented and compared to simulated surface topographies to assess the accuracy of the finite element model. Simulated surface roughness values of free surfaces in the model are also used as figures of merit for a convergence study of finite element parameters.

Keywords: Multiscale simulation; Crystal plasticity; Surface roughening; Deep drawing steel.

1 Introduction

Friction between tools and workpieces is an important consideration in the development of metal forming processes, and the roughness of finished components can influence their performance. Therefore, it is important to understand how surface topographies develop during forming. Modeling is a tool which can aid in this regard, particularly multi-scale modeling where in addition to bulk deformation of the workpiece, the deformation of individual asperities is considered. One approach to evaluate deformation on the asperity scale is the use of model asperities with a uniform geometry, and there exists a body of work both analytical [1-3], and applying finite element methods [4-6]. Conclusions from these studies offer valuable qualitative insights about the behavior of real surfaces, but quantitative findings are less transferable [7]. It is also possible to base simulated asperities on measured surface topographies to more closely match the conditions in actual forming operations [8,9].

In addition to being flattened during deformation, asperities are also formed due to the heterogeneous microstructure of polycrystals, where grains deform differently. Depending on the balance between these competing effects, the roughness of a formed sheet can be found to either increase or decrease with deformation during forming [10].

There are many considerations that affect the accuracy of finite element models of crystal plasticity. For example, different element types (e.g. tetrahedra vs. hexahedra) have been found to produce different surface topographies [11] and to have a significant influence on simulation convergence rate [12]. The number of grains in a simulated polycrystal and the number of elements per grain also have bearing on the results of crystal plasticity studies with respect to mechanical properties [13,14] and crystallographic texture development [15]. These parameters must be determined in setting up the minimum size of a representative volume element (RVE) for the material being studied.

The literature is limited with regards to determining an appropriate RVE for modeling of polycrystals where surface roughening is of interest. The aim of the present study is to evaluate a multiscale approach for modeling the roughening of a polycrystal with tensile deformation and to determine guidelines for sizing RVEs for that purpose and creating an appropriately fine mesh. Average surface height is used as the figure of merit for simulation convergence. This study was conducted along with validation tensile data from a DC04 deep drawing steel in the form of 1) stress-strain curves, 2) plastic anisotropy behavior and 3) quantitative and qualitative comparison to surface height maps for polished specimens after tensile deformation.

* Corresponding author: aidca@dtu.dk

2 Methods and procedures

This section outlines the methods used to obtain the results in the present study via physical experiments and numerical modeling.

The material used for this study was a sheet of a DC04 deep drawing steel with a thickness of 0.7 mm.

2.1 Optical microscopy

In preparation for light optical microscopy (LOM), specimens were sectioned and mounted to examine planes normal to the rolling direction (RD), transverse direction (TD), and normal direction (ND). Specimens were ground with P500, P1200, and P4000 abrasive papers, followed by polishing with 3 μm , and finally 1 μm diamond suspension. Grain boundaries were revealed via etching with nital (2% nitric acid in ethanol). Microscopy was performed using a Zeiss Axio Vert A1 Microscope. Approximate grain size in the ND was determined by counting the number of grains intersected by three lines drawn through the cross section of the specimen.

2.2 Electron backscatter diffraction

Electron backscatter diffraction (EBSD) was used to determine the crystallographic texture as well as average grain size in the rolling direction (RD) and transverse direction (TD). A specimen was ground with abrasive paper up to P4000 and electropolished with a Struers LectroPol-5 for 10 s at 31 V.

The EBSD study was conducted to examine the microstructure in the plane containing the RD and TD using a Zeiss Sigma 300 scanning electron microscope. A step size of 2 μm was used. AZtecCrystal software was used to calculate the average grain size and quantify the texture.

2.3 Tensile testing

Uniaxial tensile testing was performed to determine the mechanical properties of the DC04 steel used in this study to inform the material models for the finite element analysis. Testing was performed at room temperature using a servo mechanical press with a maximum capacity of 155 kN. Strain measurements were conducted with axial and transverse extensometers with gauge lengths of 80 mm and 20 mm, respectively, and a crosshead travel speed of 0.125 mm/s for a nominal strain rate of 0.001/s in the parallel section. Tests were performed to fracture.

Type H tensile specimens were made according to ISO 6892-1:2019 [16] with a test piece width of 20 mm, an original gauge length of 80 mm, and a parallel length of 120 mm. Specimens were cut from the parent sheets with the tensile axis oriented 0° (RD), 45°, and 90° (TD) from the rolling axis. Five replicates were tested for each orientation. For tests to determine tensile properties, specimens were left with the as-rolled finish. To examine surface roughening from deformation, one additional specimen in each of the RD and TD

orientations was manually polished with abrasive paper up to P4000 on one side and tested to 0.28 nominal strain, based on the average strain for onset of diffuse necking measured as the strain at point with the maximum load.

2.4 Surface height measurements

Surface height measurements of experimental specimens were conducted using an Olympus-LEXT confocal microscope. A 20x objective lens was used for the scans. To get a representative sample of the topography, a stitched area of 2.4 mm \times 2.4 mm was examined in a 4 \times 4 grid of images. Reported Sa values were calculated according to ISO 25178-2:2021 [17] with no filter applied.

3 Finite element modeling

The simulation of surface roughening of a polycrystal was conducted via finite element modeling (FEM). A multiscale approach was used with a continuum scale main model used to provide the boundary conditions for a submodel containing a simulated polycrystal. The FEM was conducted using Abaqus 2018, with DAMASK v2.0.2 run as an Abaqus user subroutine.

3.1 Continuum scale model

The continuum scale model used in this study was a simulation of a tensile test. The main model consisted of a cuboid model with dimensions 10 mm \times 1 mm \times 5 mm (X \times Y \times Z). As shown in Fig. 1, the tensile axis is the X direction, symmetry boundary conditions on the negative X, Y, and Z normal faces constrain the model, and an additional boundary condition in the Z direction enforces deformation consistent with the measured anisotropy of the material. The model is meshed with a hexahedral mesh with a side length of 0.05 mm to accommodate a variety of submodel sizes.

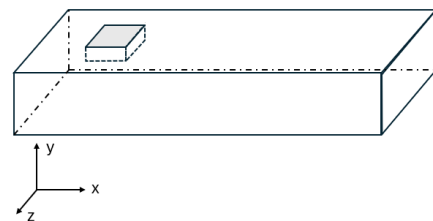


Fig. 1. Schematic illustration of main model and submodel with coordinate axes. The sample RD, ND, and TD are the model X, Y, and Z respectively. The main model has symmetry boundary conditions in the -X, -Y, and -Z directions and moving boundary conditions in +X and +Z to apply uniaxial tension. The submodel has free surfaces on the +Y and -Y faces, while the rest are submodel boundaries.

3.2 Submodel boundary conditions

The simulated polycrystal was given boundary conditions as a submodel. As shown in Fig. 1, this entailed the positive and negative X and Z normal faces following the deformation of the corresponding faces

they lay on within the main model, while the positive and negative Y normal faces were left as free surfaces.

3.3 Polycrystal generation with Neper

The tessellation of the submodel into grains was accomplished using Neper [18], version 3.3.0, a software tool for polycrystal generation and meshing. To study convergence of different sizes of volume elements (VEs), each study began with the creation of the largest size VE to be examined, with the number of grains and their aspect ratio determined from EBSD and LOM measurements. Smaller subsets of that VE were created via a Python script which redefined the borders of the model before meshing to exclude material around the edges (X and Z normal faces) and bottom (negative Y normal face) to make a smaller VE.

Texture was applied to the tessellation by using Neper's built in fiber texture to generate tessellations with a strong $\langle 111 \rangle$ //ND fiber texture with a deviation of 5° and a default tessellation with random grain orientations. These two tessellations were combined in different ratios via a Python script to achieve different intensities of the fiber texture.

For meshing, hexahedral elements were created at varying sizes using Neper's relative cell length (-rcl) attribute, and are reported here as the average number of elements per grain (total elements / total grains). Hexahedral elements were used to mesh the VE because they have been found to allow for more surface topography change for a given number of elements than tetrahedral elements [11].

3.4 DAMASK crystal plasticity model

To simulate the mechanical behavior of grains within the polycrystal, DAMASK 2.0.2 was used as an Abaqus user subroutine. In doing so, a phenomenological crystal plasticity model outlined in equation (1) and equation (2) determines the mechanical response of each grain in the polycrystal [19]. Twinning has been omitted, as the present study considers only deformation via dislocation slip.

Equation (1) describes how the shear rate for a given slip system $\dot{\gamma}^\alpha$ evolves with respect to a reference shear rate $\dot{\gamma}_0^\alpha$, resolved shear stress τ^α , and slip resistance ξ^α . Hardening is controlled by the evolution of ξ^α , which is detailed in equation (2), where ξ^α is related to the slip-slip interaction coefficient h_0^{S-S} , and for each other slip system α' , the effect of the ratio of that system's current slip resistance $\xi^{\alpha'}$ and its saturation slip resistance $\xi_\infty^{\alpha'}$, as well as the shear rate of that system $\dot{\gamma}^{\alpha'}$ and the specific slip-slip interaction parameter $h^{\alpha\alpha'}$ for the two slip systems being considered. There is also an initial slip resistance ξ_0^α dictating the slip resistance at the start of plastic deformation.

$$\dot{\gamma}^\alpha = \dot{\gamma}_0^\alpha \left| \frac{\tau^\alpha}{\xi^\alpha} \right|^n \text{sgn}(\tau^\alpha) \quad (1)$$

$$\xi^\alpha = h_0^{S-S} \cdot \sum_{\alpha'=1}^{N_S} |\dot{\gamma}^{\alpha'}| \left| 1 - \frac{\xi^{\alpha'}}{\xi_\infty^{\alpha'}} \right| \text{sgn} \left(1 - \frac{\xi^{\alpha'}}{\xi_\infty^{\alpha'}} \right) h^{\alpha\alpha'} \quad (2)$$

3.5 Mechanical property calibration

To calibrate a material model, which accurately represents the material used in the experimental work in the present study, several parameters from equations (1) and (2) were adjusted to match the experimental behavior. These were ξ_0^α to dictate the initial yield stress, ξ_∞^α to define a saturation stress, and h_0^{S-S} to control the work hardening rate.

To calibrate these values, a smaller VE was used, with a total of 200 grains, periodic in the RD. The model was strained with moving periodic boundary conditions along the tensile axis (TA//RD), implemented by extending the method proposed by Wu et al. [20] to three dimensions. The faces normal to the TD and ND were left as free surfaces. In addition to providing the average stress in the TA of the periodic faces to produce a stress-strain curve, this configuration allowed for the strain in the ND and TD to be measured in order to calculate the anisotropy coefficients for different combinations of fiber and random textures.

4 Results and discussion

4.1 Optical microscopy

An optical micrograph of the DC04 steel is shown in Fig. 2. The micrograph reveals grains of polygonal ferrite elongated in the RD. There are also clusters of particles aligned with the RD, which show up as small dark features.

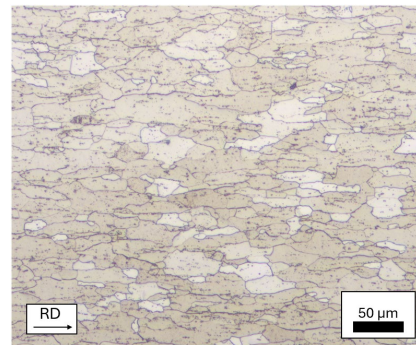


Fig. 2. Optical micrograph of DC04 in the RD-ND plane.

4.2 EBSD

Grain maps of both a physical specimen (created from EBSD data) and the top surface of a 1 mm × 1 mm VE are shown in Fig. 3, plotted with the same color key. The EBSD data show that the area fraction of the $\langle 111 \rangle$ //ND fiber texture is 55% and the average grain size is $\sim 20 \mu\text{m}$. This texture is typical of textures in rolled annealed ferritic sheet steels [21]. These features measured in the physical specimen were used as the basis for making a tessellation to match those characteristics in Neper. One notable difference is that

the simulated polycrystal has a much more uniform grain size and lacks the assortment of very large and very small grains found within the experimental material. Neper has a tool to generate grain morphologies more similar to what was measured in the DC04 specimen; however, it was unable to converge on a tessellation even for a small test VE given the other target parameters. Improving the match between grain size statistics in the real and simulated microstructures is a promising avenue of future work within this approach.

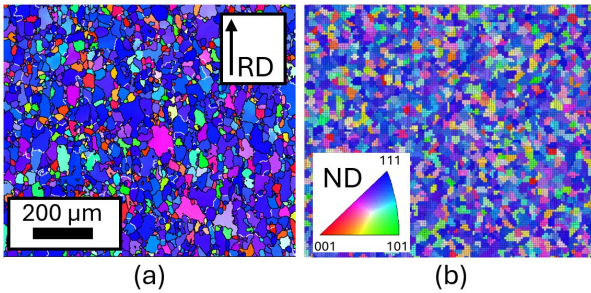


Fig. 3. Grain orientations shown (a) in the RD-TD plane of the physical specimen analyzed using EBSD, and (b) orientations in simulated polycrystal. The same scale is used for both images.

4.3 Stress-strain data

The true stress-strain curves obtained from the tensile tests are presented in Fig. 4. The greatest variation in the tensile behavior is seen for specimens tested in the TD, while specimens tested in the RD show the least variation. It is possible that this phenomenon is due to inclusions or other microstructural features of the material, which are elongated in the RD. The material does not exhibit a yield point phenomenon. Average tensile properties are shown in Table 1.

Table 1. Average tensile properties (true stresses and true strains) for the DC04 specimens.

Specimen orientation	Yield strength, 0.2% offset (MPa)	True stress at instability (MPa)	Uniform elongation (-)
RD	156	375	0.24
TD	156	368	0.23
45°	162	383	0.23

The stress-strain curve for the calibrated material model is shown alongside the experimental data for tests in the RD in Fig. 5. The simulated stress-strain curve is created from the average stress of elements in the cross section of a model with 200 grains representing a mixture of 55% $\langle 111 \rangle$ /ND fiber texture and 45% random orientations. The parameters which achieve this behavior are shown in Table 2.

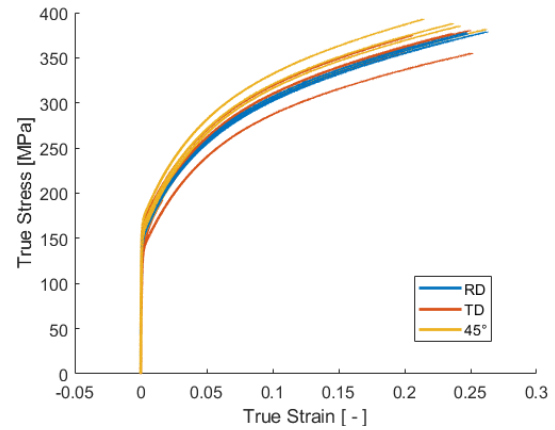


Fig. 4. True stress-strain curves for RD, TD, and 45° tensile tests ending at the instability point.

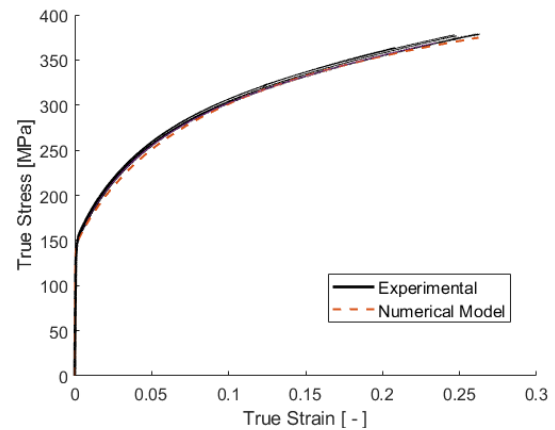


Fig. 5. Simulated and experimental stress-strain curves for uniaxial tension in the RD after calibration of the parameters in the numerical model.

Table 2. Calibrated crystal plasticity model parameters.

Parameter	Calibrated value
ξ_0^α	88 MPa
ξ_∞^α	205 MPa
h_0^{S-S}	495 MPa
C_{11}, C_{12}, C_{44}	233, 135, 118 GPa
n	20
$\dot{\gamma}_0$	0.001 /s

The anisotropy results for RD tensile tests of simulated polycrystals are presented in Fig. 6, where the anisotropy coefficient, R, for the RD is plotted against strain in the TA. There is agreement in the general behavior of the measured and simulated anisotropy behavior. Both show a sharp rise in anisotropy at low strains followed by a slow decrease at a similar slope, although the simulations predict slightly higher anisotropy values. At higher strains, experimental anisotropy begins to fall at a faster rate, however this is past the point of necking where the strain measurements of the physical specimens become less accurate as strain is no longer uniform. The tensile curves for the different fiber fractions were found to be nearly identical.

The curve with the closest match to the experimental behavior is that corresponding to a 45%

$\langle 111 \rangle$ /ND fiber (see Fig. 6). While this fraction is lower than the 55% measured experimentally, the general behavior of this cluster of curves demonstrates that the method employed is capable of producing realistic anisotropy behavior. In further simulations, the measured fiber fraction was used.

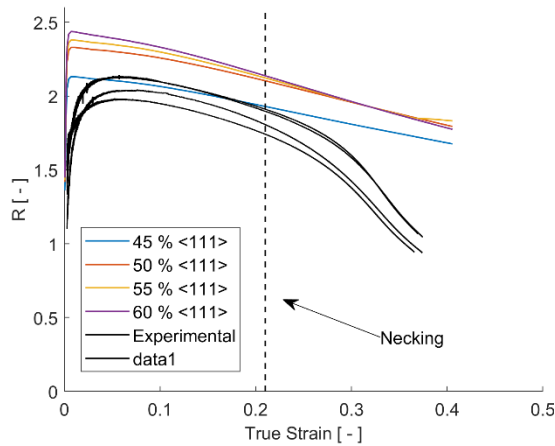


Fig. 6. Simulated and experimental anisotropy coefficient (R) as a function of true strain for tensile tests in the RD. The polycrystal models have the specified fractions of the $\langle 111 \rangle$ /ND fiber, while the rest is a random texture.

4.4 Element size study

The effect of element size on VE surface roughness is shown in Fig. 7. There is generally little difference between the surface roughness results for the different element sizes examined. Based on the results, a relative cell length of 2 was chosen for the remaining studies. This corresponds to the points with an average of 13 elements per grain. While much greater numbers of elements per grain are required to converge on expected stress-strain behavior in each grain [14], the present study finds that when the figure of merit is the average surface height, element size is not as critical.

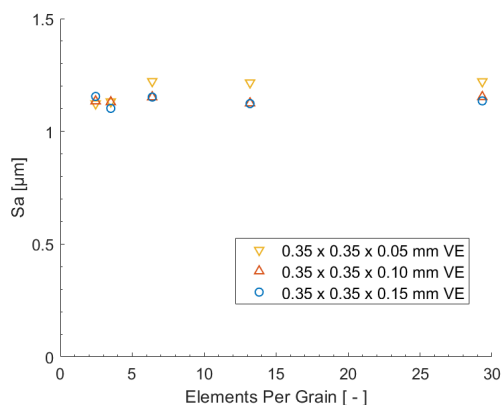


Fig. 7. Average surface roughness (Sa) vs elements per grain for RVEs of different thicknesses made from subsets of a $0.35 \text{ mm} \times 0.35 \text{ mm} \times 0.25 \text{ mm}$ polycrystal tessellation with 6380 grains.

4.5 RVE thickness study

Fig. 8 compares VE thickness to simulated surface roughness. For both VE surface areas examined, the measured surface roughness does not change

substantially with increasing VE thickness after a thickness of 12-13 grains (0.15 mm). While this is in alignment with the general consensus that roughening is dictated by grains relatively near the surface [22], it is more than the three layers of grains suggested by some studies [8, 9]. Following these results, 0.15 mm was used as the thickness for VEs in the subsequent surface area size study, so conclusions from the following work apply primarily to VEs of that thickness.

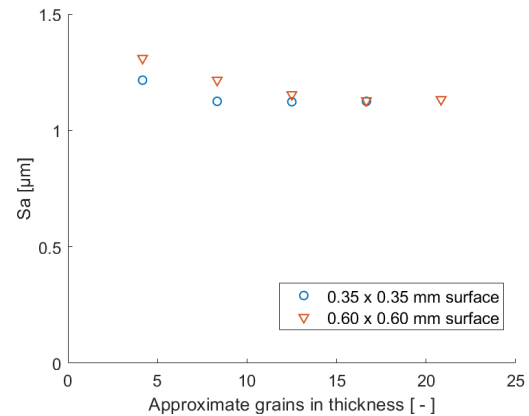


Fig. 8. Average surface roughness (Sa) vs approximate grains in thickness of VEs with a free surface of $0.6 \text{ mm} \times 0.6 \text{ mm}$ (~900 grains at the surface) made from subsets of a $0.7 \text{ mm} \times 0.7 \text{ mm} \times 0.25 \text{ mm}$ polycrystal with 25520 grains, and for subsets of a $0.35 \text{ mm} \times 0.35 \text{ mm} \times 0.25 \text{ mm}$ polycrystal with 6380 grains (~300 grains at the surface).

4.6 RVE surface area study

Plots of Sa vs starting VE surface grains for VEs reduced from initial polycrystals and measurements of portions of the RD tensile specimen of corresponding area are shown in Fig. 9. The Sa value that each study converges to and at what VE surface area that occurs varies between the different initial tessellations. This finding suggests that for smaller VE sizes, edge effects are important, indicated by all the models showing lower Sa at small sizes while the experimental measurements overshoot the converged value before leveling out. However, results from larger VE simulations suggest that the sampling of a sufficient number of grains on the surface is more important for final Sa. There is also a marked difference in roughness between experimental and simulated surfaces. This may be a grain size effect, as it has been shown that larger grains generally lead to more roughening with plastic deformation [25], and the real material contains a significant number of large grains. The simulated microstructure has the same average grain size but the default settings in Neper lead to a more uniform grain size distribution. A qualitative examination of the surface topographies may help to explain this discrepancy and is discussed in the following section.

4.7 Surface height of experimental tensile tests

Surface height plots for a portion of the experimental surface measurements and a plot from a simulated tensile test with a $0.9 \text{ mm} \times 0.9 \text{ mm} \times 0.15 \text{ mm}$ VE containing 27031 grains are shown in Fig. 10. Both the

experimental and simulated surfaces show notable roughening with islands and valleys elongated in the TA. While the general appearance is similar, there is a difference in scale both in height and in-plane. The presence of some larger grains could explain why the islands and valleys on the experimental surface are wider in addition to being taller or deeper, respectively.

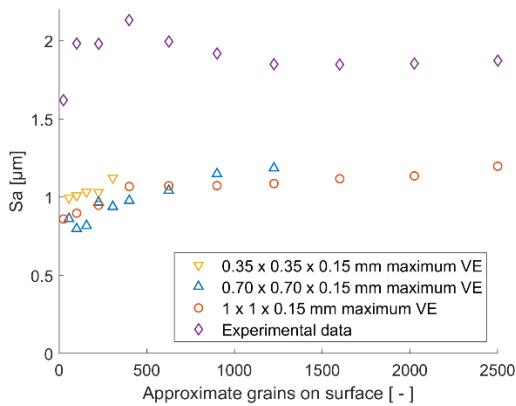


Fig. 9. Average surface roughness (S_a) vs VE side length for 0.15 mm thick VEs, which are subsets of 1.0 mm \times 1.0 mm \times 0.25 mm, 0.7 mm \times 0.7 mm \times 0.25 mm, and 0.35 mm \times 0.35 mm \times 0.25 mm polycrystals with 52082, 25520, and 6380 grains, respectively. S_a values measured from a polished specimen after tensile deformation are also included.

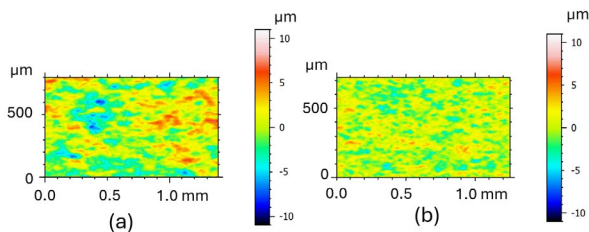


Fig. 10. Surface height maps for (a) a subsection of the measurements of a polished tensile specimen deformed in the RD, and (b) simulation of a 0.9 mm \times 0.9 mm \times 0.15 mm VE with 27031 grains. The mean surface height is 0 on the color bar.

5 Conclusions

Based on the findings presented in this study, the following conclusions are drawn:

- An RVE modeled with a phenomenological power law for crystal plasticity and a mix of fiber and random textures can closely replicate the observed stress-strain behavior and tensile anisotropy of a real deep drawing steel.
- Having enough grains exposed at the surface of the model is the primary limiting factor for the RVE size rather than the number of grains in the thickness. The results presented show that after approximately 12-13 grains through the thickness, the predicted surface roughness converges, while it takes approximately 1000 grains in area at the surface to approach convergence.
- Only a relatively small number of elements per grain are required to reach convergence of the simulated surface roughness, with approximately 10-15 elements per grain being sufficient for surface roughness convergence.

Accurately modeling grain size distribution, in addition to average size, is considered important for accurately predicting the material response.

Acknowledgements

The authors would like to thank the Independent Research Fund Denmark (grant ID 10.46540/3105-00169B) for funding of this research. The authors would also like to thank Tata Steel Europe for providing the DC04 sheet used in this study.

References

1. T. Wanheim, *Wear*, **25**, 225, (1973)
2. T. Wanheim, N. Bay, and A. S. Petersen, *Wear*, **28**, 251–258 (1974)
3. M. P. F. Sutcliffe, *Int. J. Mech. Sci.*, **30**, 847 (1988)
4. H. Ike and A. Makinouchi, *Wear*, **140**, 17 (1990)
5. Z. G. Wang, Y. Yoshikawa, T. Suzuki, and K. Osakada, *CIRP Ann.*, **63**, 277 (2014)
6. C. V. Nielsen, P. A. F. Martins, and N. Bay, *CIRP Ann.*, **65**, 261 (2016)
7. M. Zwicker, N. Bay, and C. V. Nielsen, *Discov. Mech. Eng.*, **2**, 3 (2023)
8. J. Hol, M. V. Cid Alfaro, M. B. De Rooij, and T. Meinders, *Wear*, **286**, 66 (2012)
9. M. Shisode, J. Hazrati, T. Mishra, M. De Rooij, and T. Van Den Boogaard, *Friction*, **9**, 840 (2021)
10. P. K. Saha and W. R. D. Wilson, *Wear*, **172**, no. 2, 167 (1994)
11. D. Zhao, C. Xin, T. Jin, X. Yan, S. Ma, and Z. Wang, *Eng. Comput.*, **37**, 895 (2019)
12. W. G. Feather, H. Lim, and M. Knezevic, *Comput. Mech.*, **67**, 33 (2021)
13. J. E. Bishop, J. M. Emery, R. V. Field, C. R. Weinberger, and D. J. Littlewood, *Comput. Methods Appl. Mech. Eng.*, **287**, 262 (2015)
14. H. Lim, C. C. Battaile, J. E. Bishop, and J. W. Foulk, *Int. J. Plast.*, **121**, 101 (2019)
15. Z. Zhao, S. Kuchnicki, R. Radovitzky, and A. Cuitiño, *Acta Mater.*, **55**, 2361 (2007)
16. ISO 6892-1, (2019)
17. ISO 25178, (2021)
18. R. Quey, P. R. Dawson, and F. Barbe, *Comput. Methods Appl. Mech. Eng.*, **200**, 1729 (2011)
19. F. Roters *et al.*, *Comput. Mater. Sci.*, **158**, 420 (2019)
20. W. Wu, J. Owino, A. Al-Ostaz, and L. Cai, *SIMULIA Community Conf. Proc.*, 707 (2014)
21. S. Schreijäg, *KIT Dissertation*, (2012).
22. A. V. Panin *et al.*, *Phys. Mesomech.*, **15**, 94 (2012)
23. Y. Wu, V. Recklin, and P. Groche, *J. Manuf. Mater. Process.*, **5**, Art. no. 2 (2021)
24. O. Zinovieva, V. Romanova, R. Balokhonov, A. Zinoviev, and Z. Kovalevskaya, *J. Appl. Math. Phys.*, **2**, Art. no. 6 (2014)
25. D. V. Wilson, W. T. Roberts, and P. M. B. Rodrigues, *Metall. Trans. A*, **12**, 1595 (1981)